Research Article

Amphiphilic Polymer-Modified Uniform CuFeSe$_2$ Nanoparticles for CT/MR Dual-Modal Imaging

Min Wu,[1,2] Shaozhi Fu ⓘ,[3] Jian Shu ⓘ,[1] and Kequan Yu[4]

[1]*Department of Radiology, The Affiliated Hospital of Southwest Medical University, Luzhou, Sichuan, China*
[2]*Department of Radiology, People's Hospital of Chongqing Yubei District, Yubei District, Chongqing, China*
[3]*Department of Oncology, The Affiliated Hospital of Southwest Medical University, Luzhou, Sichuan, China*
[4]*Department of Surgery, The First Affiliated Hospital of Chongqing Medical University, Chongqing, China*

Correspondence should be addressed to Shaozhi Fu; shaozhifu513@163.com and Jian Shu; shujiannc@163.com

Recently, magnetic photothermal nanomaterials have attracted much attention in the diagnosis and treatment of cancer. In this study, we developed the ultrasmall magnetic CuFeSe$_2$ nanoparticles for CT/MR dual-modal imaging. By controlling the reaction time and condition, CuFeSe$_2$ nanoparticles were synthesized by a simple directly aqueous method. After modification with copolymer methoxy polyethylene glycol-polycaprolactone (MPEG-PCL), the obtained MPEG-PCL@CuFeSe$_2$ nanoparticles showed excellent water solubility, colloidal stability, and biocompatibility. In addition, they also exhibited superparamagnetism and X-ray's characteristics. For these properties, they will become ideal nanomaterials for CT/MR dual-modal imaging.

1. Introduction

In recent years, nanotechnology has been widely used in the field of biomedicine, such as the development of tumor therapeutic drugs and molecular imaging probes [1, 2]. Among them, semiconductor nanomaterials not only have strong fluorescence characteristics but also have fine and uniform particle size, while carbon dots and organic polymer fluorescent nanomaterials have low biological toxicity and relatively stable chemical properties [3, 4]. Many fluorescent nanomaterials, for example, gold-based nanomaterials [5, 6], carbon-based nanomaterials [7], conjugated polymeric nanomaterials [8], and graphene [9–11], are extensively used in photoacoustic imaging and photothermal therapy of tumors, which achieve the purpose of the integration of diagnosis and treatment of tumors.

CuFeSe$_2$ is classified as I-III-VI$_2$ ternary chalcogenide semiconductor materials, which has interesting optical, electronic, and magnetic properties. Until now, many studies about CuFeSe$_2$ mainly focus on the synthesis methods as well as magnetic and optoelectronic properties [12–16]. There are few reports about its application in diagnosis and cancer treatment

[17, 18]. Therefore, we will try to explore the potential value of its application in the field of imaging diagnosis.

Currently, the CuFeSe$_2$ nanostructures can be prepared by the solvothermal reaction [19] and the high-temperature solid phase reaction [16]. The products which are often synthesized tend to have a nonuniform size and are prone to agglomeration. Therefore, in an effort to overcome their disadvantages of CuFeSe$_2$ nanostructures, we attempted to prepare with biodegradable copolymer loaded CuFeSe$_2$ nanocrystals to increase the solubility in aqueous media.

MPEG-PCL is an amphiphilic copolymer, and many studies demonstrate that MPEG-PCL copolymer can significantly improve water solubility of hydrophobic drugs and keep better stability [20–22]. Therefore, it can be used to load CuFeSe$_2$ nanoparticles for molecular imaging in vivo. First, the properties of PCL, such as crystallinity, tensile strength, and hydrophobicity, can be easily modulated, and thus, the loading capacity for hydrophobic CuFeSe$_2$ nanoparticles can be tuned. Second, PEG is nonimmunogenic and highly hydrophilic [23]. Surface coating with PEG can prolong nanoparticle circulation time in vivo, leading to better-enhanced imaging results.

Every imaging modality has its strengths and weaknesses [24]. For instance, X-ray computed tomography (CT) owns its advantages, such as fast acquisition time, large tissue penetration depth, and high spatial resolution, but it has a poor soft-tissue contrast. Magnetic resonance (MR) imaging possesses favorable spatial and soft-tissue resolution, and it can implement multisequence, multiparameter imaging, but its limitation is low sensitivity. Nuclear imaging techniques, including single photon emission computed tomography (SPECT) and positron emission tomography (PET), exhibit high sensitivity and are quantitative, but along with a poor spatial resolution. However, multimodal imaging can improve the accuracy of cancer diagnosis by combining two or more imaging modalities into one system [25, 26]. It overcomes the intrinsic limitations of single modality.

In this study, the ultrasmall magnetic $CuFeSe_2$ nanostructures were prepared by a simple direct aqueous method. After modification with methoxy polyethylene glycol-polycaprolactone (MPEG-PCL), the biosafety of obtained MPEG-PCL@$CuFeSe_2$ nanoparticles was evaluated. Lastly, the X-ray attenuation property and T_2 MR relaxometry of MPEG-PCL@$CuFeSe_2$ NPs in vitro/in vivo were measured to explore the potential application of these NPs as dual-modal CT/MR imaging contrast agents.

2. Experimental Section

2.1. Materials.
Copper (II) chloride dihydrate ($CuCl_2 \cdot 2H_2O$, ≥99%), ferrous (II) sulfate heptahydrate ($FeSO_4 \cdot 7H_2O$, ≥99%), selenium powder (Se, ≥99.5%), sodium borohydride ($NaBH_4$, 99%), L-cysteine (cys, ≥99%), ε-caprolactone (ε-CL, Alfa Aesar, USA), poly(ethylene glycol) methyl ether (MPEG, Mn = 2000, Aldrich, USA), and stannous octoate ($Sn(Oct)_2$) were bought from Sigma-Aldrich (USA).

2.2. Synthesis of $CuFeSe_2$ Nanoparticles.
For the synthesis of $CuFeSe_2$ nanoparticles, 78.96 mg of Se powder was dispersed in 100 mL of Milli-Q water, and then 75.60 mg of $NaBH_4$ was added to reduce it at ambient conditions with protection of nitrogen flow for one hour. After Se powder was completely reduced, a colorless solution is obtained. A 10 mL mixture of $CuCl_2$ $2H_2O$ (85.24 mg), $FeSO_4$ $7H_2O$ (139.01 mg), and L-cysteine (121.20 mg) was separately prepared, and then the above mixture was added into the selenium precursor solution immediately to form a black solution. The resultant solution was collected after centrifugation with a speed of 3500 rpm for twenty minutes to remove impurities. The purified $CuFeSe_2$ solution was stored at 4°C for further characterization and application.

2.3. Functionalization of $CuFeSe_2$ Nanoparticles.
Methoxy poly (ethylene glycol)-poly (ε-caprolactone) (MPEG-PCL) used in this study was synthesized by ring-opening polymerization of ε-CL on MPEG using $Sn(Oct)_2$ as catalyst, according to a previous report [27]. The MPEG-PCL colloidal solution was prepared by liquid rotary evaporation method.

For functionalization of $CuFeSe_2$ nanoparticles, the above purified $CuFeSe_2$ solution was slowly added into the MPEG-PCL colloidal solution under ultrasonication for 4 hours, and then the MPEG-PCL-modified $CuFeSe_2$ nanoparticles were obtained after centrifugation to remove excess and large impurities. The purified MPEG-PCL@$CuFeSe_2$ solution was stored at 4°C for future experiments.

2.4. Characterization.
The hydrodynamic diameters and zeta potentials of prepared $CuFeSe_2$ solution and MPEG-PCL@$CuFeSe_2$ solution were measured by dynamic light scattering (DLS, NanoBrook 90Plus Zeta, Brookhaven, USA) at 25°C. The size and morphology of prepared $CuFeSe_2$ nanoparticles and MPEG-PCL@$CuFeSe_2$ nanoparticles were characterized with a transmission electron microscope (TEM, Tecnai G2 F20, USA). The crystallography structures of $CuFeSe_2$ nanoparticles and MPEG-PCL@$CuFeSe_2$ nanoparticles were characterized by using an X-ray diffractometer equipped with Cu Kα radiation ($\lambda = 0.15406$ nm). A scanning rate of 0.1°/s was applied to record the pattern in the 2θ range of 10–90°. The T2-weighted images of MPEG-PCL@$CuFeSe_2$ at different concentrations were scanned under a 3T clinical MRI scanner at room temperature. After the T2-weighted MR images were acquired, the signal intensity was measured by a manually drawn region-of-interest for each sample.

2.5. Cell Culture and Cytotoxicity Assessment.
4T1 murine breast cancer cells, A549 human lung adenocarcinoma, and human normal liver cells were cultured in standard cell media supplemented with 10% fetal bovine serum (FBS) and antibiotics (100 U/mL penicillin and 100 μg/mL streptomycin) at 37°C in an atmosphere of 5% CO_2. All cell culture-related reagents were purchased from HyClone (USA). The cytotoxicity of MPEG-PCL-$CuFeSe_2$ NPs was evaluated by the MTT assay. The cells were first seeded into 96-well plates (1×10^4 cells per well) and cultured for 24 h and then added into different concentrations of MPEG-PCL-$CuFeSe_2$ and continued to culture for 24 h. After this, 10 μL MTT (5 mg/mL) was added. Four hours later, the supernatant medium was removed, and 150 μL DMSO was added into each well to dissolve the resulting formazan crystals. The absorbance was measured at 490 nm using a spectrophotometric microplate reader (iMark, MA, USA). The cytotoxicity was calculated as the percentage of cell viability.

2.6. Animal Model.
We acquired female BALB/c mice (6–8 weeks of age, 25–30 g of weight) from Chongqing Tengxin Biotechnology Co. Ltd. (Chongqing, China). To generate the 4T1 tumor murine model, 1×10^6 cells in the 100 μL serum-free RMPI-1640 medium were subcutaneously injected into in the right side thigh root of each mouse. All mice were selected for imaging experiments when their tumors grew to 80 mm³.

2.7. In Vitro CT/MR Dual-Modality Imaging. Various concentrations of MPEG-PCL@CuFeSe$_2$ solution were dispensed in 5.0 mL Eppendorf tubes for CT and MR contrast imaging. The MR imaging for in vitro study was performed on a 3.0 T clinical magnetic resonance (MR) scanner (PHILIPS, Holland). The representative imaging parameters of the T2-weighted images were as follows: repetition time (TR) = 5348 ms, echo time (TE) = 70 ms, slice thickness = 1.5 mm, slice spacing = 0.15 mm, matrix = 256 × 256 pixels, field of view (FOV) = 30 cm × 60 cm × 25 cm, NSA = 4, and flip angle = 10°. The region-of-interest was selected by drawing manually to measure the signal intensity of MPEG-PCL@CuFeSe$_2$ solution from the T2-weighted MR images. The CT data were acquired using a clinical CT imaging scanner (GE, USA), and X-ray attenuation values for all samples were finally calculated in Hounsfield units (HU) by averaging over the region-of-interest (ROI). CT imaging parameters were as follows: tube current = 600 mA, tube voltage = 100 kV, and slice thickness = 0.625 mm.

2.8. In Vivo CT/MR Dual-Modality Imaging. The 4T1 tumor-bearing mice were acquired before and after intratumorally (i.t.) injected with MPEG-PCL@CuFeSe$_2$ (250 μL, 2 mg/mL) and imaged with a 3.0 T clinical magnetic resonance (MR) scanner (PHILIPS, Holland) equipped with a small animal coil. The representative imaging parameters of the T2-weighted images were as follows: repetition time (TR) = 5348 ms, echo time (TE) = 70 ms, slice thickness = 1.5 mm, slice spacing = 0.15 mm, matrix = 256 × 256 pixels, field of view (FOV) = 30 cm × 60 cm × 25 cm, NSA = 4, and flip angle = 10°. The region-of-interest in the tumor area of each mouse was selected by drawing manually to measure the signal intensity of tumors from the T2-weighted MR images. The CT images were acquired before and after intratumorally (i.t.) injected with MPEG-PCL@CuFeSe$_2$ (250 μL, 2 mg/mL) on a clinical CT imaging scanner (GE, USA), and the CT imaging parameters were as follows: tube current = 600 mA, tube voltage = 100 kV, and slice thickness = 0.625 mm. The region-of-interest in the tumor area of each mouse was selected by drawing manually to measure the CT value of tumors from the CT images.

2.9. In Vivo Toxicity Study. The major organs/tissues were taken from mice after intravenous injection of MPEG-PCL@CuFeSe$_2$ (a dose of 20 mg/kg) at 1 day, 3 days, 7 days, and 15 days postinjection, while other mice without injection were used as the control group (four mice per group). Then, the obtained major organs/tissues were fixed in 4% formalin, paraffin-embedded, sectioned, and stained with hematoxylin & eosin (H&E) and then imaged by using a digital microscope to evaluate the histological changes.

3. Results and Discussion

3.1. Synthesis and Characterizations of MPEG-PCL@CuFeSe$_2$ Nanoparticles. In our experiments, MPEG-PCL@CuFeSe$_2$ nanoparticles with uniform sizes and morphologies were synthesized by a simple direct aqueous method. The resultant nanoparticles were characterized by transmission electron microscopy (TEM) to determine their size and morphology. Small spherical particles with a size of 4.2 ± 0.7 nm are clearly observed (Figures 1(a), 1(c)). The crystal structure of CuFeSe$_2$ nanoparticles was observed by their high-resolution TEM (HR-TEM) image, which clearly shows the lattice fringes with an interplanar spacing of 0.325 nm (Figure 1(b)). The FTIR spectra showed a typical variation peak of C=O at 1727.60 cm^{-1} and typical variation peaks of C-H at 2891.05 cm^{-1} and 2949.12 cm^{-1} in the MPEG-PCL@CuFeSe$_2$ nanoparticles, verifying the successful modification of MPEG-PCL (Figure 2(a)).

The X-ray powder diffraction (XRD) results show that both CuFeSe$_2$ and MPEG-PCL-CuFeSe$_2$ nanoparticles have crystal face peaks at (112) and (220), indicating that the nanoparticles are cubic crystal structures (Figure 2(b)). The content of MPEG-PCL polymer on the surfaces of CuFeSe$_2$ nanoparticles was determined by thermogravimetric analysis (TGA) to be approximately 40.0 wt. % (Figure 2(c)), and the TGA results demonstrate the successful coating of CuFeSe$_2$ nanoparticles with MPEG-PCL. For the magnetic properties of CuFeSe$_2$ and MPEG-PCL@CuFeSe$_2$ nanoparticles, the superparamagnetic properties of CuFeSe$_2$ and MPEG-PCL@CuFeSe$_2$ were illustrated by the absence of a hysteresis loop in the field-dependent magnetization measurement (Figure 2(d)). According to the results from DLS, the hydrodynamic diameters of MPEG-PCL NPs and MPEG-PCL@CuFeSe2 NPs were 25.31 ± 2.07 nm and 120.91 ± 3.44 nm, respectively. MPEG-PCL NPs had a negative surface charge of −21.03 ± 1.53 mV, and MPEG-PCL@CuFeSe2 NPs had a negative surface charge of −10.85 ± 2.59 mV (Table 1).

3.2. Toxicity Studies of MPEG-PCL@CuFeSe$_2$ Nanoparticles. Good biosecurity is an important criterion for measuring whether nanomaterials can be applied to living organisms. Thus, in vitro MTT assay and in vivo pathological assay were investigated to test the cytotoxicity and biosecurity of MPEG-PCL@CuFeSe$_2$ NPs, respectively. The results of MTT assay showed that the viability of the above three kinds of cells still kept above 90% in the concentration range of 0–150 μg/mL for MPEG-PCL@CuFeSe$_2$ nanoparticles after cultured 24 h, demonstrating the cytotoxicity is not obvious (Figure 3(a)). In order to test toxicity study of MPEG-PCL@CuFeSe$_2$ NPs in vivo, histological assessment of tissues was performed to determine whether MPEG-PCL@-CuFeSe$_2$ NPs caused damage to important organs. The above representative organs including heart, liver, spleen, lung, and kidney had no apparent histopathological abnormalities or lesions, compared with those of the control group throughout the entire study. Therefore, the results of in vivo toxicity indicated the good biocompatibility of MPEG-PCL@CuFeSe$_2$ NPs (Figure 3(b)).

3.3. In Vitro CT/MR Dual-Modality Imaging. We successfully performed in vitro CT/MR imaging experiment, and it demonstrates the potential of MPEG-PCL@CuFeSe$_2$ NPs in
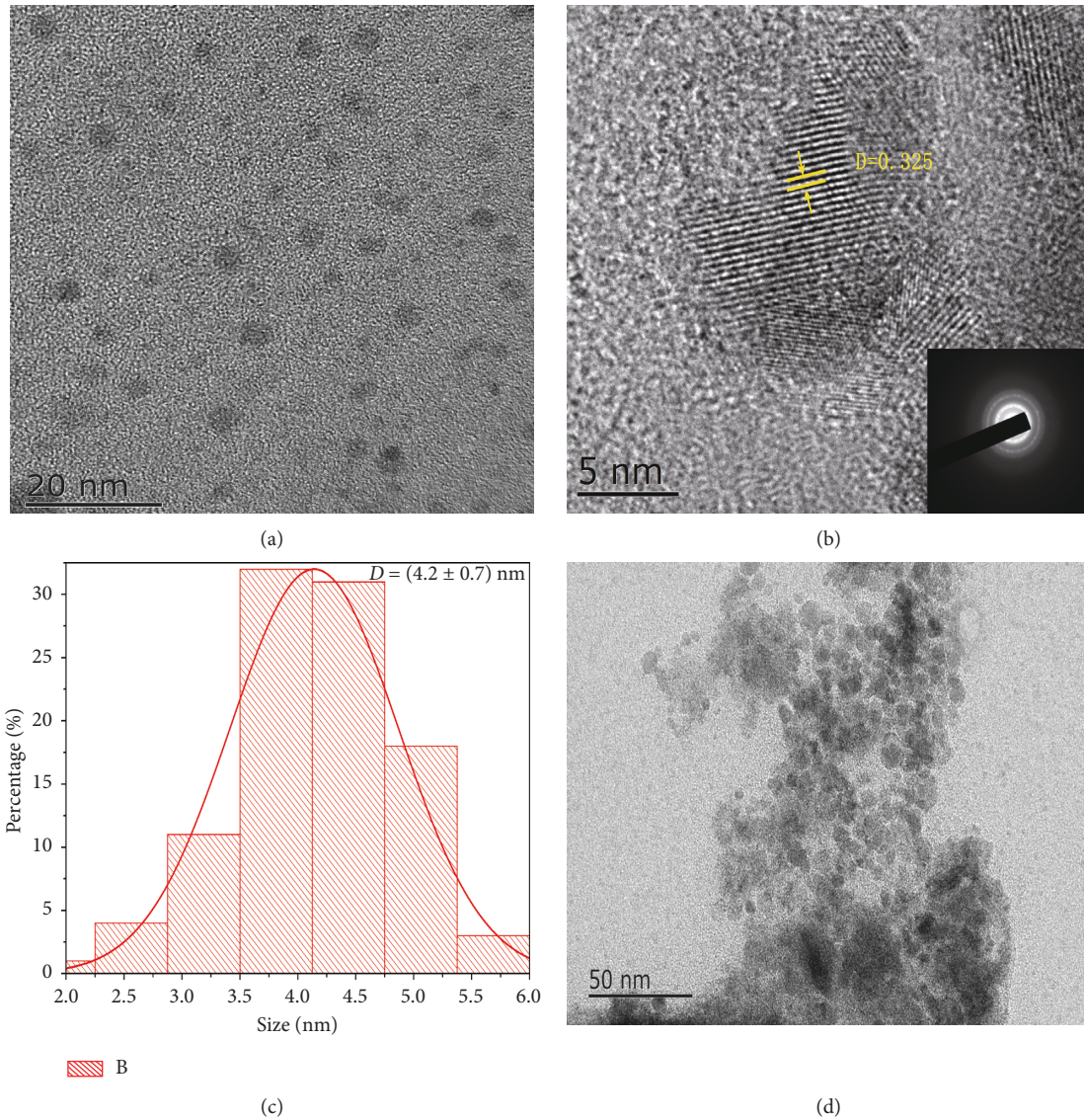
(a)

(b)

(c)

(d)

FIGURE 1: Characterization of as-prepared $CuFeSe_2$ and MPEG-PCL@$CuFeSe_2$ NPs. (a) TEM image of $CuFeSe_2$. (b) HRTEM image with corresponding SAED pattern (inset). (c) The histogram for the measured particle size distribution. (d) TEM image of MPEG-PCL@$CuFeSe_2$.

CT/MR imaging. As shown in Figure 4(a), from the CT images and Hounsfield unit (HU) values of different concentrations of MPEG-PCL@$CuFeSe_2$ NPs in comparison with the clinically used iopromide (Omnipaque, General Electric Pharmaceutical Industry, Shanghai China), with the increasement of the concentration of MPEG-PCL@$CuFeSe_2$ NPs and iopromide, the CT signal intensity was gradually enhanced, and at the same concentration, the images are brighter when MPEG-PCL@$CuFeSe_2$ NPs are compared with the clinically used iopromide. In addition, the in vitro MRI imaging performance of MPEG-PCL@$CuFeSe_2$ NPs

was evaluated with a clinically used 3.0 T MRI instrument. Figure 4(b) shows T_2-weighted images of MPEG-PCL@$CuFeSe_2$ NPs. With the increasing concentration of MPEG-PCL@-$CuFeSe_2$ NPs, the MR signal intensity was gradually decreasing, resulting in getting darker images.

3.4. In Vivo CT/MR Dual-Modality Imaging. Based on the in vitro dual-modal CT/MR contrast performance and good biocompatibility, we performed in vivo CT/MR imaging experiments of mPEG-PCL@$CuFeSe_2$ nanoparticles in
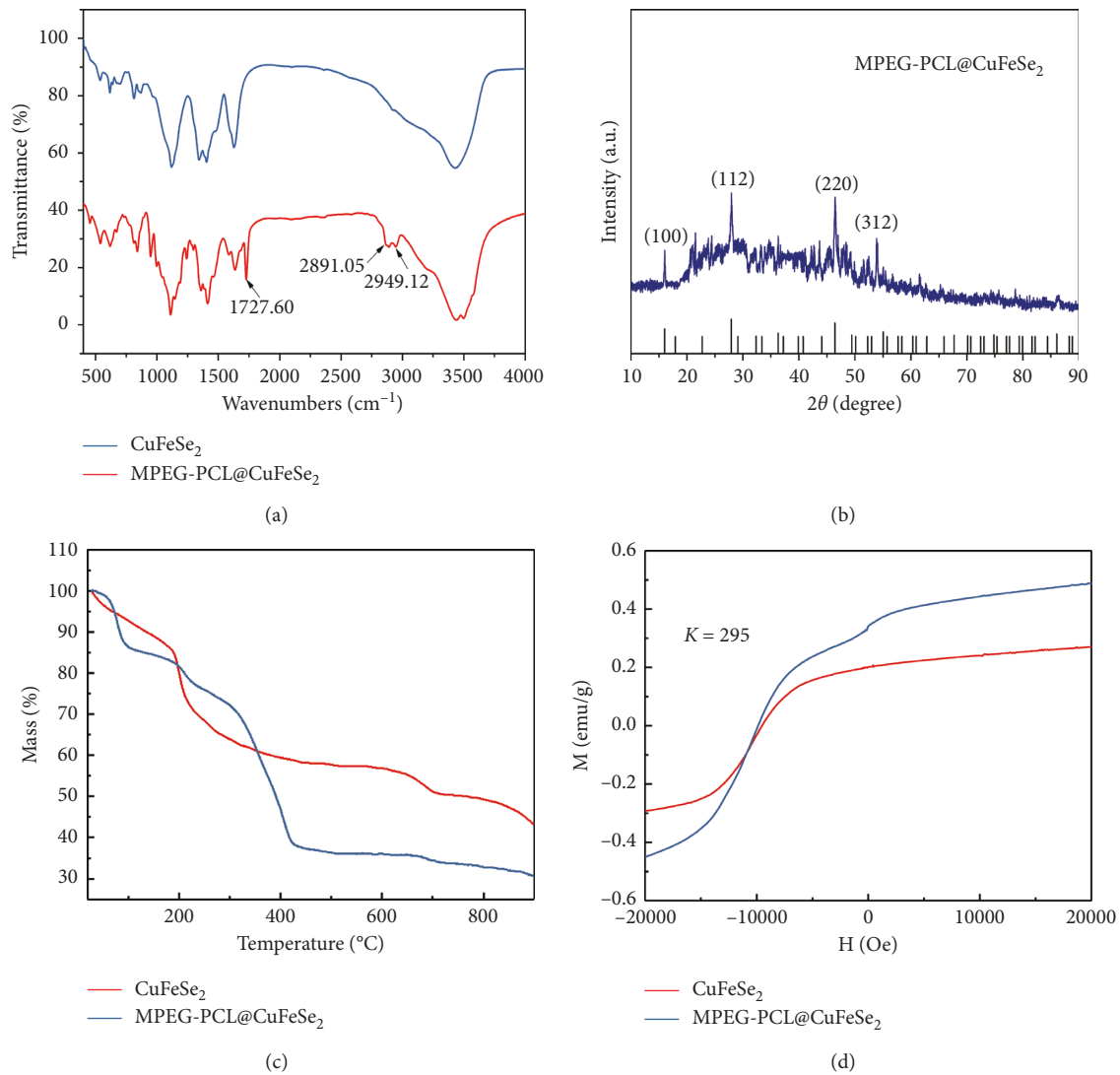
Figure 2: (a) FTIR spectra of CuFeSe$_2$ and MPEG-PCL@CuFeSe$_2$ NPs. (b) XRD patterns of CuFeSe$_2$ prepared with and without MPEG-PCL in comparison with the standard peaks of cubic berzelianite (JCPDS card no. 81-1959). (c) TGA curve of CuFeSe$_2$ and MPEG-PCL@CuFeSe$_2$ NPs. (d) Magnetization plot of CuFeSe$_2$ and MPEG-PCL@CuFeSe$_2$ NPs as a function of the applied field at 295K.

Table 1: Hydrodynamic diameters and zeta potentials of NPs.

Nanoparticles	Diameters (d/nm)	PDI	Zeta potential (φ/mv)
MPEG-PCL	25.31 ± 2.07	0.263 ± 0.527	-21.03 ± 1.53
MPEG-PCL@CuFeSe2	120.91 ± 3.44	0.183 ± 0.007	-10.85 ± 2.59

PDI: polydispersity index.

transplanted mice. In the first place, CT images were acquired before and after intratumoral injection, and the tumor sites showed an enhancement with a higher CT value after administration of contrast agent when compared with those before injection (Figure 5(a)). Similar to CT imaging, MR images were acquired before and after intratumoral injection, and the tumor sites showed an enhancement with a lower T$_2$WI MR signal intensity after administration of contrast agent when compared with those before injection (Figure 5(d)). The above results indicate the development of MPEG-PCL@CuFeSe$_2$ has the potential to target bimodal CT/MR imaging.
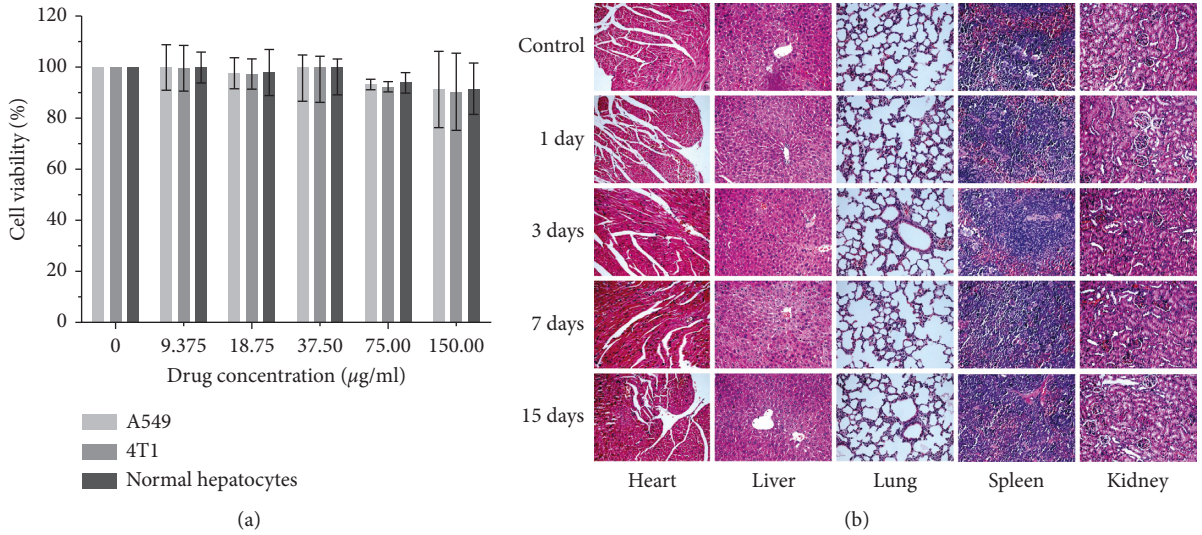
(a)

(b)

FIGURE 3: (a) Cytotoxicity studies on 4T1, A549, and human normal liver cells after 24 h incubation with mPEG-PCL@CuFeSe$_2$ NPs at different concentrations. (b) Representative H&E stained images of major organs including the heart, liver, spleen, lung, and kidney collected from the tumor-bearing mice at various timepoints after the injection of mPEG-PCL@CuFeSe$_2$ NPs, in comparison with those of healthy mice. No obvious organ damage or lesions were observed after treatment.
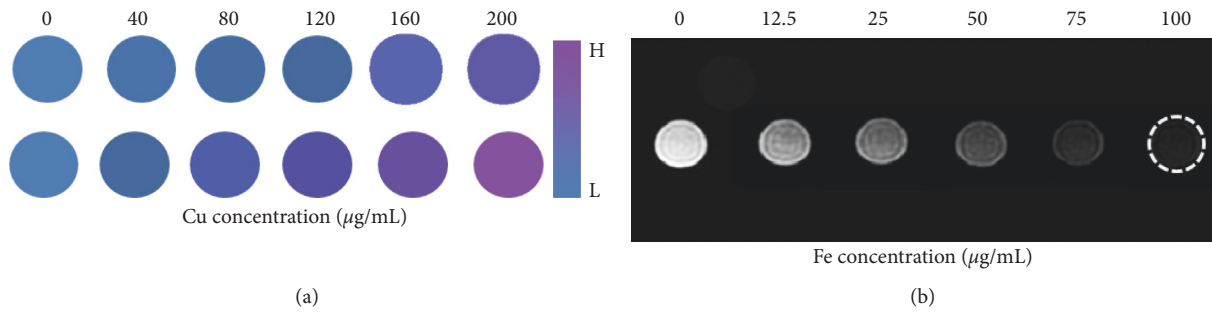

(a)

(b)

FIGURE 4: (a) The CT images of mPEG-PCL@CuFeSe$_2$ NPs at different concentrations. (b) The T$_2$-weighted MR images of mPEG-PCL@-CuFeSe$_2$ NPs at different Fe concentrations.
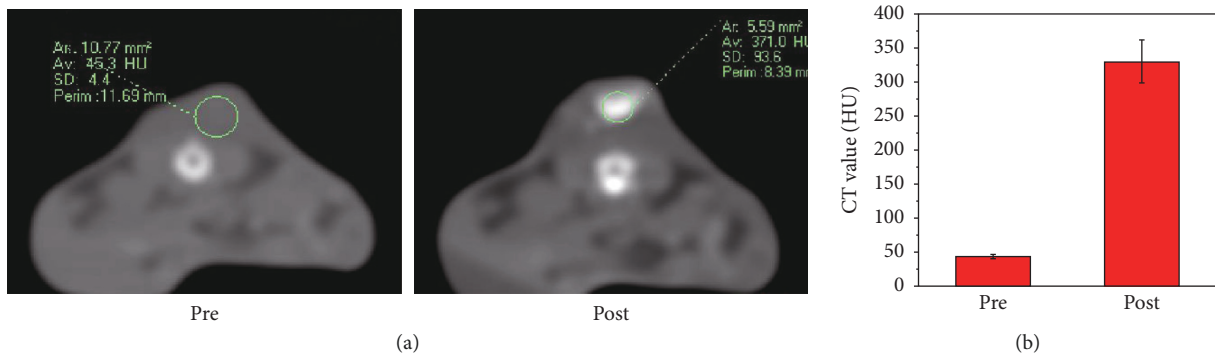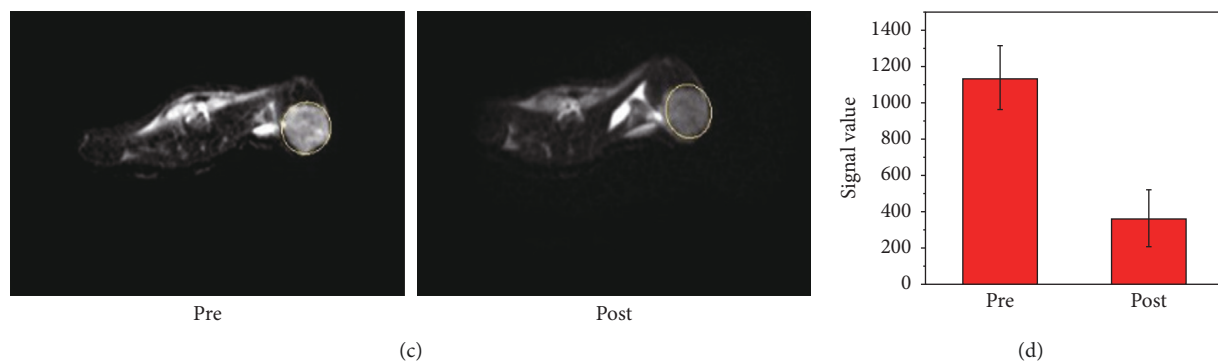

(a)

(b)

FIGURE 5: Continued.

Figure 5: (a, b) CT images and CT values of mice collected pre- and post-intratumoral injection of mPEG-PCL@CuFeSe$_2$ NPs. (c, d) T$_2$-weighted MR images and signal intensity of mice collected pre- and post-intratumoral injection of mPEG-PCL@CuFeSe$_2$ NPs.

4. Conclusions

In summary, the MPEG-PCL copolymer-modified CuFeSe$_2$ nanoparticles with favorable biological safety were successfully prepared by an environmentally friendly aqueous route under ambient conditions, and the MPEG-PCL@CuFeSe$_2$ nanoparticles perform positive CT/MR contrast effect in vitro/in vivo. These excellent properties enable them to be a promising nanotheranostic agent for in vivo multimodal imaging.

Data Availability

The laboratory experimental data used to support the findings of this study are available from the first author upon request.

Conflicts of Interest

The authors declare that they have no conflicts of interest.

Acknowledgments

References

[1] L. Cheng, J. Liu, X. Gu et al., "PEGylated WS2Nanosheets as a multifunctional theranostic agent for in vivo dual-modal CT/photoacoustic imaging guided photothermal therapy," *Advanced Materials*, vol. 26, no. 12, pp. 1886–1893, 2014.

[2] M. Zhou, R. Zhang, M. Huang et al., "A chelator-free multifunctional [64Cu]CuS nanoparticle platform for simultaneous micro-PET/CT imaging and photothermal ablation therapy," *Journal of the American Chemical Society*, vol. 132, no. 43, pp. 15351–15358, 2010.

[3] A. Dzik-Jurasz, C. Domenig, M. George et al., "Diffusion MRI for prediction of response of rectal cancer to chemoradiation," *The Lancet*, vol. 360, no. 9329, pp. 307-308, 2002.

[4] D.-M. Koh, E. Scurr, D. Collins et al., "Predicting response of colorectal hepatic metastasis: value of pretreatment apparent diffusion coefficients," *American Journal of Roentgenology*, vol. 188, no. 4, pp. 1001–1008, 2007.

[5] F. Jabeen, M. Najam-ul-Haq, R. Javeed, C. Huck, and G. Bonn, "Au-nanomaterials as a superior choice for near-infrared photothermal therapy," *Molecules*, vol. 19, no. 12, pp. 20580–20593, 2014.

[6] R. Ahmad, J. Fu, N. He, and S. Li, "Advanced gold nanomaterials for photothermal therapy of cancer," *Journal of Nanoscience and Nanotechnology*, vol. 4880, pp. 67–80, 2016.

[7] C. Cha, S. R. Shin, N. Annabi, M. R. Dokmeci, and A. Khademhosseini, "Carbon-based nanomaterials: multifunctional materials for biomedical engineering," *ACS Nano*, vol. 7, no. 4, pp. 2891–2897, 2013.

[8] Y. Shi, M. Liu, F. Deng et al., "Recent progress and development on polymeric nanomaterials for photothermal therapy: a brief overview," *Journal of Materials Chemistry B*, vol. 5, no. 2, 2016.

[9] K. Yang, L. Hu, X. Ma et al., "Multimodal imaging guided photothermal therapy using functionalized graphene nanosheets anchored with magnetic nanoparticles," *Advanced Materials*, vol. 24, no. 14, pp. 1868–1872, 2012.

[10] S. Wang, Q. Zhang, X. F. Luo et al., "Magnetic graphene-based nanotheranostic agent for dual-modality mapping guided photothermal therapy in regional lymph nodal metastasis of pancreatic cancer," *Biomaterials*, vol. 35, no. 35, pp. 9473–9483, 2014.

[11] S. Gao, L. Zhang, G. Wang et al., "Hybrid graphene/Au activatable theranostic agent for multimodalities imaging guided enhanced photothermal therapy," *Biomaterials*, vol. 79, no. 3, pp. 36–45, 2016.

[12] J. M. Delgado, G. D. de Delgado, M. Quintero, and J. C. Woolley, "The crystal structure of copper iron selenide, CuFeSe2," *Materials Research Bulletin*, vol. 27, no. 3, pp. 367–373, 1992.

[13] J. Lamazares, F. Gonzalez-Jimenez, E. Jaimes et al., "Magnetic, transport, X-ray diffraction and Mössbauer measurements on CuFeSe2," *Journal of Magnetism and Magnetic Materials*, vol. 104–107, no. 12, pp. 997-998, 1992.

[14] J. C. Bernede, N. Hamdadou, and A. Khelil, "X-ray photoelectron spectroscopy study of CuFeSe2 thin films," *Journal of Electron Spectroscopy and Related Phenomena*, vol. 141, no. 1, pp. 61–66, 2004.

[15] L. V. Kradinova, A. M. Polubotko, V. V. Popov, V. D. Prochukhan, Y. V. Rud, and V. E. Skoriukin, "Novel zero-gap compounds, magnetics: CuFeS2and CuFeTe2,"

Semiconductor Science and Technology, vol. 8, no. 8, p. 1616, 1993.

[16] Y.-K. Hsu, Y.-G. Lin, and Y.-C. Chen, "One-pot synthesis of CuFeSe2 cuboid nanoparticles," *Materials Research Bulletin*, vol. 46, no. 11, pp. 2117–2119, 2011.

[17] X. Jiang, S. Zhang, F. Ren et al., "Ultrasmall magnetic CuFeSe2 ternary nanocrystals for multimodal imaging guided photo-thermal therapy of cancer," *ACS Nano*, vol. 11, no. 6, pp. 5633–5645, 2017.

[18] W. Dang, T. Li, B. Li et al., "A bifunctional scaffold with CuFeSe2 nanocrystals for tumor therapy and bone reconstruction," *Biomaterials*, vol. 160, pp. 92–106, 2018.

[19] Q. Lu, J. Hu, K. Tang, B. Deng, Y. Qian, and Y. Li, "The synthesis of CuFeSe2 through a solventothermal process," *Journal of Crystal Growth*, vol. 217, no. 3, pp. 271–273, 2000.

[20] M. S. Kim, H. Hyun, K. S. Seo et al., "Preparation and characterization of MPEG–PCL diblock copolymers with thermo-responsive sol–gel–sol phase transition," *Journal of Polymer Science Part A Polymer Chemistry*, vol. 44, no. 18, pp. 5413–5423, 2006.

[21] B. L. Wang, Y. M. Shen, Q. W. Zhang et al., "Codelivery of curcumin and doxorubicin by MPEG-PCL results in improved efficacy of systemically administered chemotherapy in mice with lung cancer," *International Journal of Nanomedicine*, vol. 8, no. 1, p. 3521, 2013.

[22] H. Kheiri Manjili, P. Ghasemi, H. Malvandi, M. S. Mousavi, E. Attari, and H. Danafar, "Pharmacokinetics and in vivo delivery of curcumin by copolymeric mPEG-PCL micelles," *European Journal of Pharmaceutics and Biopharmaceutics*, vol. 116, pp. 17–30, 2017.

[23] E. Blanco, C. W. Kessinger, B. D. Sumer, and J. Gao, "Multifunctional micellar nanomedicine for cancer therapy," *Experimental Biology and Medicine*, vol. 234, no. 2, pp. 123–131, 2009.

[24] R. Weissleder and U. Mahmood, "Molecular imaging," *Radiology*, vol. 219, no. 2, pp. 316–333, 2001.

[25] D.-E. Lee, H. Koo, I.-C. Sun, J. H. Ryu, K. Kim, and I. C. Kwon, "Multifunctional nanoparticles for multimodal imaging and theragnosis," *Chemical Society Reviews*, vol. 41, no. 7, pp. 2656–2672, 2012.

[26] P. Padmanabhan, A. Kumar, S. Kumar, R. K. Chaudhary, and B. Gulyás, "Nanoparticles in practice for molecular-imaging applications: an overview," *Acta Biomaterialia*, vol. 41, pp. 1–16, 2016.

[27] L. Chen, X. Ni, H. Zhang et al., "Preparation, characterization, in vitro and in vivo anti-tumor effect of thalidomide nanoparticles on lung cancer," *International Journal of Nanomedicine*, vol. 13, pp. 2463–2476, 2018.